AIP | Physics of Plasmas

Effect of compressibility on the Rayleigh–Taylor and Richtmyer–Meshkov instability induced nonlinear structure at two fluid interface

M. R. Gupta, Sourav Roy, Manoranjan Khan, H. C. Pant, Susmita Sarkar, and M. K. Srivastava

Citation: Physics of Plasmas (1994-present) **16**, 032303 (2009); doi: 10.1063/1.3074789
View online: http://dx.doi.org/10.1063/1.3074789
View Table of Contents: http://scitation.aip.org/content/aip/journal/pop/16/3?ver=pdfcov
Published by the AIP Publishing

Effect of compressibility on the Rayleigh–Taylor and Richtmyer–Meshkov instability induced nonlinear structure at two fluid interface

M. R. Gupta,[1,a)] Sourav Roy,[1,b)] Manoranjan Khan,[1,c)] H. C. Pant,[1] Susmita Sarkar,[2,d)] and M. K. Srivastava[3]
[1]*Department of Instrumentation Science and Centre for Plasma Studies, Jadavpur University, Kolkata 700032, India*
[2]*Department of Applied Mathematics, University of Calcutta, Kolkata 700009, India*
[3]*Theoretical Physics Division, Bhaba Atomic Research Centre, Mumbai 400085, India*

(Received 2 September 2008; accepted 6 January 2009; published online 5 March 2009)

The effect of compressibility and of density variation on Rayleigh–Taylor and Richtmyer–Meshkov instability of the temporal development of two fluid interfacial structures such as bubbles and spikes have been investigated. It is seen that the velocity of the tip of the bubble or spike increases (destabilization) if the local Atwood number increases due to density variation of either of the fluids. The opposite is the result, i.e., the bubble or spike tip velocity decreases (stabilization) if the density variation leads to lowering of the value of the local Atwood number. The magnitude of stabilization or destabilization is an increasing function of the product of the wave number k and interfacial pressure p_0. The effect of compressibility is quite varied. If the heavier (upper) fluid alone is incompressible $(\gamma_h \to \infty)$, but the lighter fluid is compressible the growth rate is higher (destabilization) than when both the fluids are incompressible. Moreover the heavier fluid remaining incompressible the growth rate decreases (stabilization) as γ_l (finite) increases and ultimately tends to the incompressible limit value as $\gamma_l \to \infty$. With $\gamma_l \to \infty$ but γ_h finite the growth increases (destabilization) as γ_h increases. When both γ_h and γ_l are finite (density $\rho_h >$ density ρ_l) the growth is reduced when $\gamma_h < \gamma_l$ compared to that when both fluids are incompressible and enhanced when $\gamma_h > \gamma_l$. The set of nonlinear equations describing the dynamics of bubbles and spikes in the presence of fluid density variations are not analytically integrable in closed form. The results derived by numerical solution methods are represented and interpreted in corresponding figures. © *2009 American Institute of Physics*. [DOI: 10.1063/1.3074789]

I. INTRODUCTION

The Richtmyer–Meshkov instability (RMI) which develops when a shock wave passes an interface between two fluids or the Rayleigh–Taylor instability (RTI) which occurs when a heavier fluid overlies a lighter one in the field of gravity are of importance in a variety of physical phenomena such as inertial confinement fusion or supernova remnant formation. The interface perturbation leads to development of fingerlike structures in the nonlinear stage. The structure is termed a bubble or a spike according as the lighter or the heavier fluid penetrates into the heavier or lighter fluid. The dynamics of the instability of two constant density fluids and the associated nonlinear structure has been studied by several authors[1–6] using an expression near the tip of the bubble or the spike up to second order in the transverse coordinate following Layzer's approach.[7] The study was extended to include the effect of purely temporal density variation on the Rayleigh–Taylor instability of a fluid supported against a fluid of extremely low (almost vanishing) density.[8]

The effect of compressibility on the growth rate of Rayleigh–Taylor instability was investigated earlier by several authors[9–13] within the domain of linear theory. Lezzi and Prosperetti[9] concluded that compressibility has negligible effect on the growth rate both for sufficiently small $(k \to 0)$ and for sufficiently large $(k \to \infty)$ wave numbers in the case of adiabatically stratified fluids. For intermediate value of k, however, it is no longer negligible. The compressibility effect was found to be one of the responsible factors for stabilization or destabilization according as the lighter fluid is compressible while the heavier one is of uniform density or the opposite. Moreover, it was found that if the heavier fluid is incompressible the growth rate decreases as the adiabatic exponent γ_l of the lighter fluid increases. If the lighter fluid is incompressible the growth rate increases as γ_h increases. When both fluids are compressible and $\rho_h > \rho_l$, growth rate is higher when $\gamma_h > \gamma_l$ than when $\gamma_l > \gamma_h$. Somewhat different conclusions were arrived at elsewhere;[10,11] compressibility can either enhance or reduce the linear growth rate depending on the relative magnitude of the sound speeds in the two media.[11–13]

The effect becomes more pronounced as the adiabatic exponent decreases from $\gamma = \infty$ to $\gamma = 1$ (isothermal stratification case)[10] and this again increases with k.

In this paper, we have relaxed the restriction of constant density in RMI and RTI in the nonlinear regime. Even the assumptions of isentropic pressure-density relationship $p = \kappa\rho^{\gamma}$ introduces important modification. The Atwood num-

[a)]Electronic mail: mrgupta_cps@yahoo.co.in.
[b)]Electronic mail: sourav_royju@yahoo.com.
[c)]Electronic mail: mkhan_ju@yahoo.com. Telephone: +91-33-24146414. Fax: +91-33-24137902.
[d)]Electronic mail: susmita62@yahoo.co.in.

ber $A=(\rho_h-\rho_l)/(\rho_h+\rho_l)$ changes to $A^*=(\rho_h^*-\rho_l^*)/(\rho_h^*+\rho_l^*)$ where $\rho_m^*=(1-1/\gamma_m)\rho_m$ ($m=h,l$ according as the fluid is heavier or lighter). If $\gamma_h<\gamma_l$ where $\rho_h>\rho_l$ (this happens in many cases, e.g., SF_6-air, CO_2-air, air-He) one finds $A^*<A$. This alone affects the stability in the sense that the asymptotic bubble tip velocity $\sqrt{(2/3)[A/(1+A)](g/k)}$ reduces to $\sqrt{(2/3)[A^*/(1+A^*)](g/k)}$.[5] We have also taken into account the density variation of the fluids. When the fluid is no longer incompressible, the work function p/ρ in Bernoulli's equation describing the dynamics of RMI and RTI for constant density, is replaced by $\int(dp/\rho)\approx[\gamma/(\gamma-1)](p_0/\rho_0)[1+(\gamma-1)(\delta\rho/\rho_0)]$; here p_0 and ρ_0 denote the unperturbed pressure and density at the interface and $\delta\rho$ denotes density variation. The above simple relation shows that the effect of compressibility can be approximately incorporated by introducing an extra work function proportional to the surface pressure p_0 (in effect the usual sound speed $\gamma p_0/\rho_0$) and density gradient scale length as $(\delta\rho/\rho_0)\approx[(1/\rho_0)(\delta\rho/\delta y)]\delta y$ (y is in the direction normal to unperturbed surface). Thus the degree of stabilization or destabilization (depending on the algebraic sign of the density gradient at the surface) will be proportional to the interfacial pressure p_0. A similar conclusion was made earlier in the linear theory investigation of RTI.[14]

Section II briefly presents the kinematic boundary conditions; the latter being fluid density independent are the same as in earlier publications. The density variation affects the dynamical boundary condition. This is introduced in Sec. III which subsequently presents the modified set of temporal growth equations describing instabilities. It is interesting to note the similarity of the present set of equations (in absence of density variation) with the phenomenological buoyancy-drag model equation.[15–17] The results based on numerical solution of the instability equations and their discussion are contained in Sec. IV.

It is shown in Sec. IV A that if the initial state of the lighter fluid is one of the decompression while the heavier fluid is incompressible ($\gamma_h\to\infty$) the growth is enhanced but it is reduced if the initial state is one of compression. On the other hand if the lighter fluid is incompressible ($\gamma_l\to\infty$) while the upper fluid is compressible the foregoing results hold but in reverse order. This is seen in Sec. IV B. Such possibility of nonlinear growth rate enhancement or depression depending on the compression or decompression of the initial state bears resemblance to an earlier result[8] obtained recently. Our results, however, apply both to RTI and RMI to the interface of two fluids of finite density. In Sec. IV C it is seen that the nonlinear growth rate decreases with increasing γ_l if the heavier fluid is incompressible while it increases with decreasing compressibility of the heavier fluid (increasing γ_h). Further with $\rho_h>\rho_l$, the growth rate with $\gamma_h>\gamma_l$ is greater than that for incompressible fluids and lower if $\gamma_h<\gamma_l$. In this respect the compressibility effect is qualitatively similar to that in linear theory.[9] In Sec. IV D is discussed the dependence on wave number k and sound speed in the two fluids. Finally the results are summarized in Sec. V.

II. KINEMATIC BOUNDARY CONDITION

Assume that the undisturbed surface is $y=0$, the transverse coordinate being represented by x. The heavier fluid (density ρ_h) occupies the region $y>0$ while the lighter fluid (density ρ_l) is in the region $y<0$; gravity is taken to point along the negative y-axis. The finger shaped interface perturbation is taken to have a parabolic form

$$y(x,t)\equiv\eta(x,t)=\eta_0(t)+\eta_2(t)x^2. \tag{1}$$

Corresponding to the above stated assumption regarding the region occupied by the heavier and lighter fluids we have the following:

$$\eta_0>0,\quad \eta_2<0 \quad \text{for the bubble}, \tag{2}$$

$$\eta_0<0,\quad \eta_2>0 \quad \text{for the spike}. \tag{3}$$

Following Goncharov[5] the velocity potential describing the irrotational motion for the heavier and lighter fluids are assumed to be given by

$$\phi_h(x,y,t)=a_1(t)\cos(kx)e^{-k[y-\eta_0(t)]};\quad y>0, \tag{4}$$

$$\phi_l(x,y,t)=b_0(t)y+b_1(t)\cos(kx)e^{k[y-\eta_0(t)]};\quad y<0. \tag{5}$$

The introduction of three unknown functions [two first harmonics $a_1(t)$ and $b_1(t)$ and one zeroth harmonic $b_0(t)$] are required to equalize the total number of equations obtained form the kinematical and boundary conditions describing the dynamics. This was pointed out earlier by Hecht *et al.*[1]

With the above choice the velocity potentials given by Eqs. (4) and (5) we have

$$\text{div}\,\vec{v}_{h,l}=-\nabla^2\phi_{h,l}=0. \tag{6}$$

Thus we have assumed the fluctuations (of the fluid velocity) to be incompressible. However this does not require that the fluid itself is incompressible.[18] The continuity equation becomes convective; the total time derivative

$$\frac{D\rho_{(h,l)}}{Dt}=\frac{\partial\rho}{\partial t}+\vec{v}_{(h,l)}\cdot\vec{\nabla}\rho_{(h,l)}=0. \tag{7}$$

We now turn to the kinematic boundary conditions corresponding to interfacial surface perturbation given by Eq. (1):

$$(v_h)_x\eta_x-(v_h)_y=(v_l)_x\eta_x-(v_l)_y, \tag{8}$$

$$\eta_t+(v_h)_x\eta_x=(v_h)_y. \tag{9}$$

Substituting in Eqs. (8) and (9) for $\eta(x,t)$ from Eq. (1) and for $(v_{h,l})_x$ and $(v_{h,l})_y$ from Eqs. (4) and (5), expanding in powers of the transverse coordinate x neglecting terms $O(x^i)$ ($i\geq 3$) we obtain the following relations:

$$\frac{d\xi_1}{dt}=\xi_3, \tag{10}$$

$$\frac{d\xi_2}{dt}=-3\xi_3\left(\xi_2+\frac{1}{6}\right), \tag{11}$$

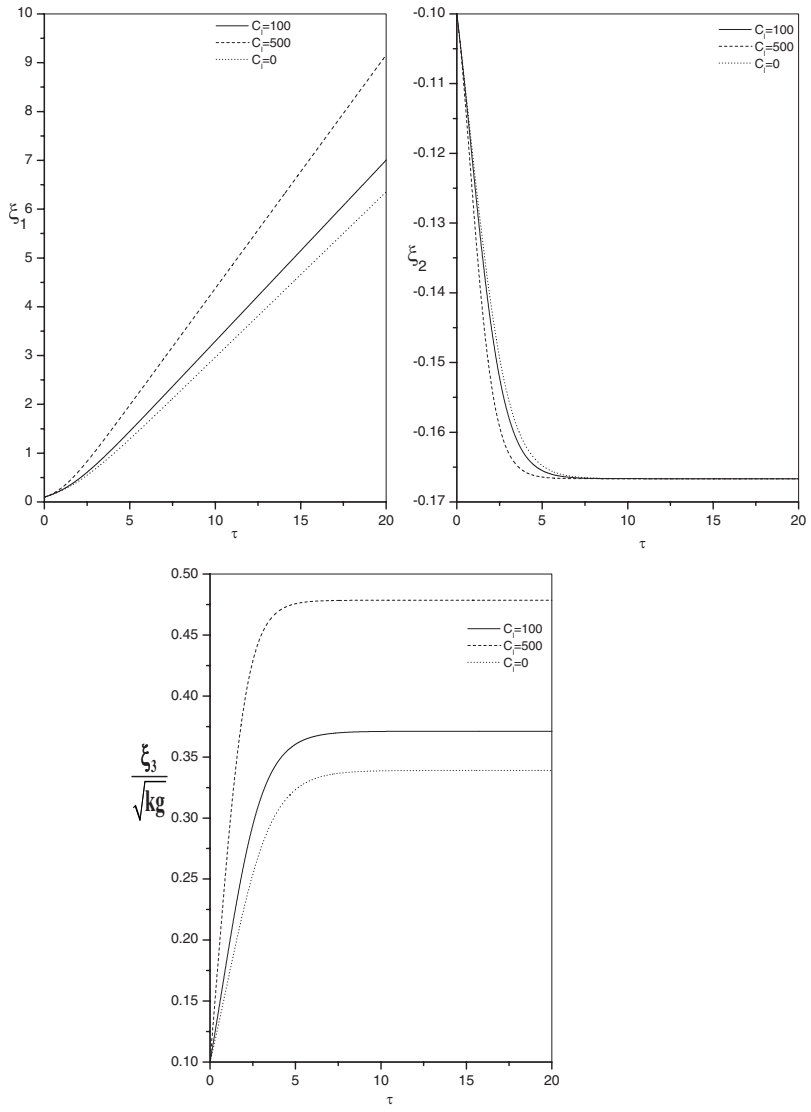

FIG. 1. The graph represents the solution of the set of equations (37) for $C_l=0$, 100, and 500 with initial values $\xi_1=0.1$, $\xi_2=-0.1$, and $\xi_3/\sqrt{kg}=0.1$, $\rho_{l1}(t=0)/\tilde{\rho}_{l0}=0.001$ (decompression) and $r^*=1.5262$. The result shows growth rate enhancement for bubble (RTI).

$$b_0 = \frac{-6\xi_2}{3\xi_2 - \frac{1}{2}} k a_1, \tag{12}$$

$$b_1 = \frac{3\xi_2 + \frac{1}{2}}{3\xi_2 - \frac{1}{2}} a_1, \tag{13}$$

where

$$\xi_1 = k\eta_0; \quad \xi_2 = \eta_2/k; \quad \xi_3 = k^2 a_1. \tag{14}$$

ξ_1 and ξ_2 are, respectively, the nondimensionalized (with respect to the wave length) displacement and curvature of the tip of the nonlinear structure and ξ_3/k is its velocity.

Equations (10)–(13) are equivalent to the kinematic boundary conditions and are the same as obtained earlier[4–6] as Eqs. (8) and (9) are independent of fluid compressibility.

III. DYNAMICAL BOUNDARY CONDITION WITH COMPRESSIBILITY EFFECT

We now analyze the dynamical boundary condition incorporating the effect of compressibility. The condition of fluid homogeneity being relaxed the equation of continuity of the heavier fluid occupying the region $y>0$ and satisfying $\vec{\nabla}\cdot\vec{v}_h=0$ is convective:

$$\frac{\partial \rho_h}{\partial t} - \vec{\nabla}\phi_h \cdot \vec{\nabla}\rho_h = 0. \tag{15}$$

To satisfy Eq. (15) with $\vec{v}_h$ given by Eq. (4) we set

$$\rho_h(x,y,z,t) = \rho_{h0}(t) + \rho_{h1}(t)\cos(kx)e^{-k[y-\eta_0(t)]} \tag{16}$$

in Eq. (15) leading to

$$\dot{\rho}_{h0} + (\dot{\rho}_{h1} + k\dot{\eta}_0\rho_{h1})\cos(kx)e^{-k(y-\eta_0)} - k^2 a_1 \rho_{h1} e^{-2k(y-\eta_0)} = 0. \tag{17}$$

Corresponding to the interfacial structure represented by Eq. (1) the foregoing equation yields on equating coefficients of

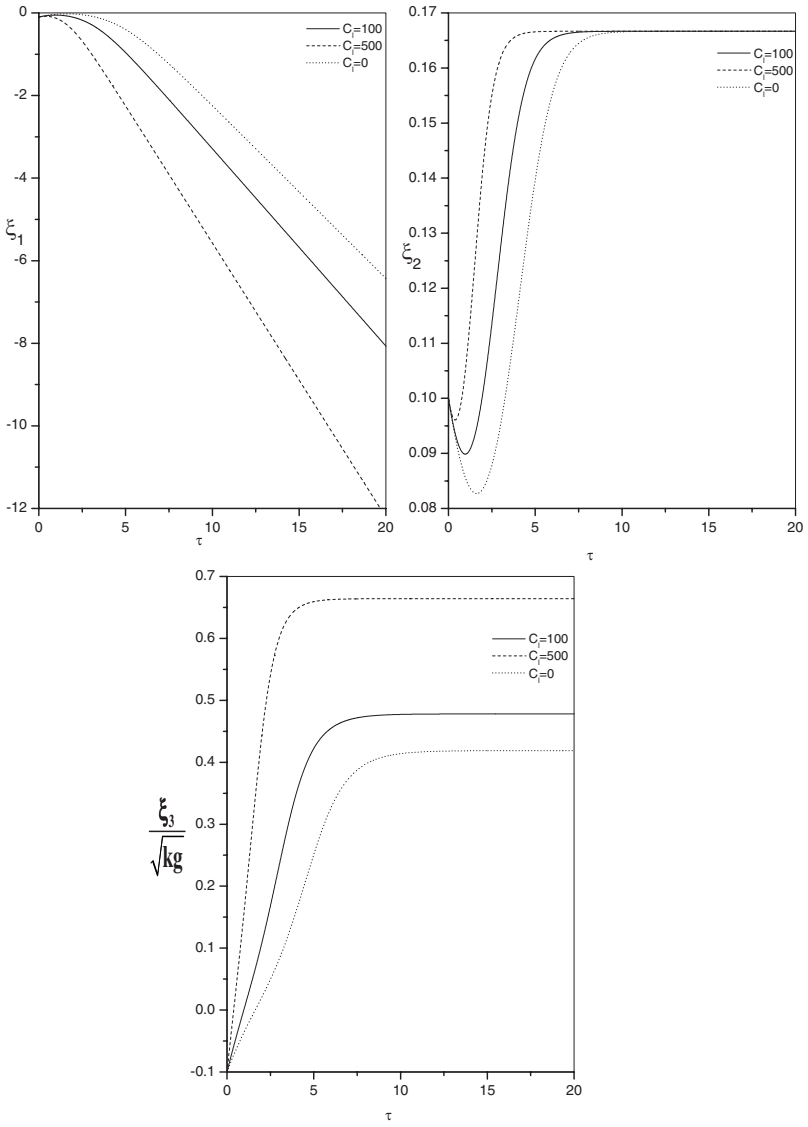

FIG. 2. The same for spikes considering initial values $\xi_1=0.1$, $\xi_2=-0.1$, $\xi_3/\sqrt{kg}=0.1$, $\rho_{l1}(t=0)/\tilde{\rho}_{l0}=0.001$ (decompression), and $r^*=1.5262$. The result shows growth rate enhancement for spikes (RTI).

x^r $(r=0,2)$ and neglecting terms $O(x^r)$ $(r>2)$

$$\dot{\rho}_{h0}+\dot{\rho}_{h1}=0,$$

giving

$$\rho_{h0}(t)+\rho_{h1}(t)=\tilde{\rho}_{h0}, \tag{18}$$

a constant, and

$$\frac{\dot{\rho}_{h1}}{\rho_{h1}}=\frac{\xi_2-\frac{1}{2}}{\xi_2+\frac{1}{2}}. \tag{19}$$

In obtaining Eqs. (18) and (19) we have made use of relation $\dot{\xi}_1=k\dot{\eta}_0=k^2a_1$ [Eq. (14)]. So the density $\rho_h(x,y,t)$ as represented in Eq. (16) reduces to the following expression:

$$\rho_h(x,y,t)=\tilde{\rho}_{h0}-k^2\rho_{h1}(t)\left(\xi_2+\tfrac{1}{2}\right)x^2 \quad \text{to} \quad O(x^r) \quad r\geq 3. \tag{20}$$

Similarly the equation of continuity of lighter fluid which fills up the region $y<0$ is

$$\frac{\partial\rho_l}{\partial t}-\vec{\nabla}\phi_l\cdot\vec{\nabla}\rho_l=0. \tag{21}$$

With ϕ_l given by Eq. (5) and ρ_l taken in the form

$$\rho_l(x,y,z,t)=\rho_{l0}(t)+\rho_{l1}(t)\cos(kx)e^{k[y-\eta_0(t)]} \tag{22}$$

and proceeding as before we obtain

$$\dot{\rho}_{l0}+\dot{\rho}_{l1}=0.$$

Consequently

$$\rho_{l0}(t)+\rho_{l1}(t)=\tilde{\rho}_{l0}, \tag{23}$$

a constant, and the expression for the density of the lighter fluid on the perturbed surface $y=\eta_0(t)+\eta_2(t)x^2$ becomes

$$\rho_l(x,y,t)=\tilde{\rho}_{l0}+k^2\rho_{l1}(t)\left(\xi_2-\tfrac{1}{2}\right)x^2 \tag{24}$$

to $O(x^2)$. Substituting for $\rho_l(x,y,t)$ in Eq. (21) and equating coefficient of x^2 it follows that

$$\frac{\dot{\rho}_{l1}}{\rho_{l1}}=\frac{\xi_2+\frac{1}{2}}{\xi_2-\frac{1}{2}}\frac{\xi_2+\frac{1}{6}}{\xi_2-\frac{1}{6}}\xi_3. \tag{25}$$

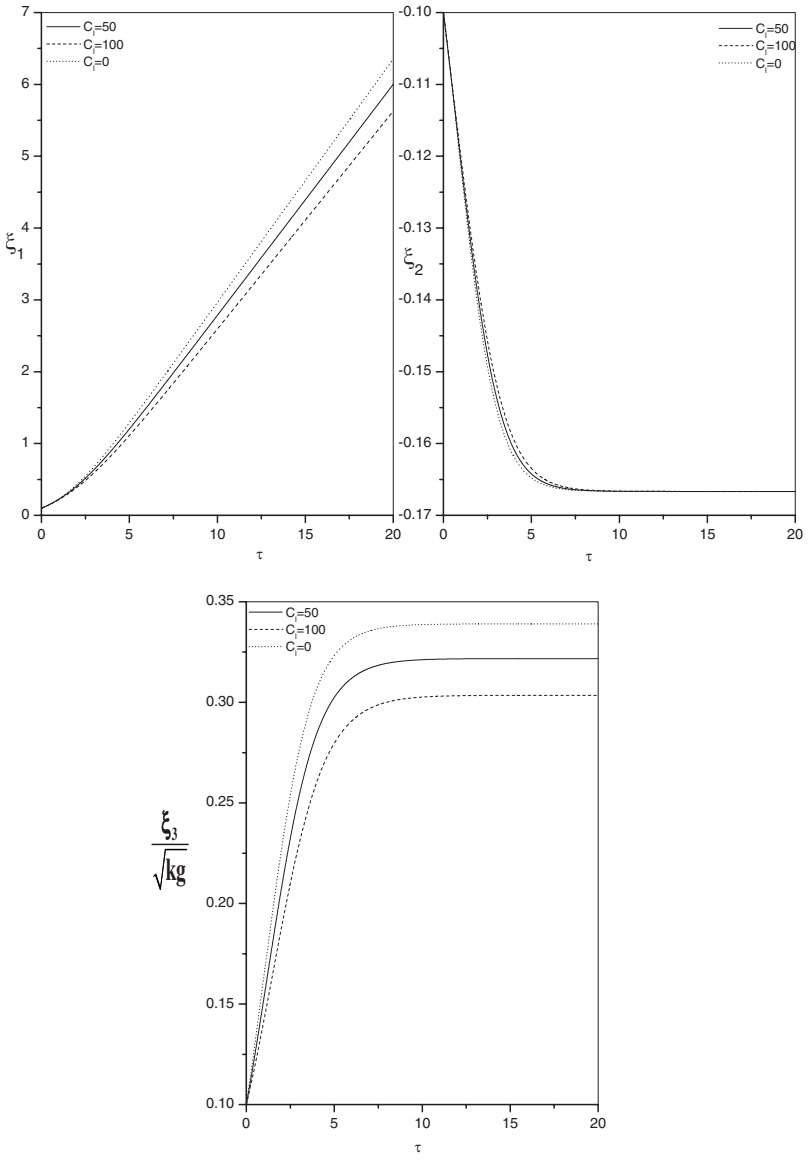

FIG. 3. The graph represents the solution of the set of equations (37). C_l=0, 50, and 100. Initial values same as in Fig. 1 $\rho_{l1}(t=0)/\tilde{\rho}_{l0}=-0.001$. Growth rate depression for bubbles (RTI).

The interfacial boundary conditions are the same as for constant density fluid. The dynamical boundary condition is, however, modified. For the heavier fluid Bernoulli's equation is

$$-\frac{\partial \phi_h}{\partial t}+\frac{1}{2}(\vec{\nabla}\phi_h)^2=-gy-\int\frac{dp_h}{\rho_h}+f_h(t). \tag{26}$$

Corresponding to uniform density the fluid pressure induced potential (work) function is p_h/ρ_h ($=p_hV_h$ where V_h is the specific volume); for adiabatic equation of state it turns out to be

$$\int\frac{dp_h}{\rho_h}=\frac{\gamma_h\kappa_h}{\gamma_h-1}[\rho_h(x,y,t)]^{\gamma_h-1}=\frac{\gamma_h}{\gamma_h-1}\frac{p_{h0}}{\tilde{\rho}_{h0}}\left[1-\frac{\rho_{h1}(t)}{\tilde{\rho}_{h0}}k^2\left(\xi_2+\frac{1}{2}\right)x^2\right]^{\gamma_h-1}, \tag{27}$$

the last relation follows on employing Eq. (20) and using the expression for undisturbed state pressure at the heavier fluid interface, i.e., $p_{h0}=\kappa_h(\tilde{\rho}_{h0}^{\gamma})$. Similarly in case of lighter fluid we have on using Eq. (24)

$$\int\frac{dp_l}{\rho_l}=\frac{\gamma_l}{\gamma_l-1}\frac{p_{l0}}{\tilde{\rho}_{l0}}\left[1+\frac{\rho_{l1}(t)}{\tilde{\rho}_{l0}}k^2\left(\xi_2-\frac{1}{2}\right)x^2\right]^{\gamma_l-1}, \tag{28}$$

where $p_{l0}=\kappa_l(\tilde{\rho}_{l0})^{\gamma_l}$ is the undisturbed fluid pressure at the lighter fluid interface.

The dynamical boundary condition which provides the third companion of the kinematic boundary conditions (10) and (11) is obtained by using the undisturbed state relation

$$p_{h0}=p_{l0}\quad(=p_0,\ \text{say}) \tag{29}$$

together with representative equations (19) and (25) of the continuity equations of heavier and lighter fluids. This completes the system and is described by the compressibility dependent temporal evolution of the bubble or spike structures of the two fluid interface as given below

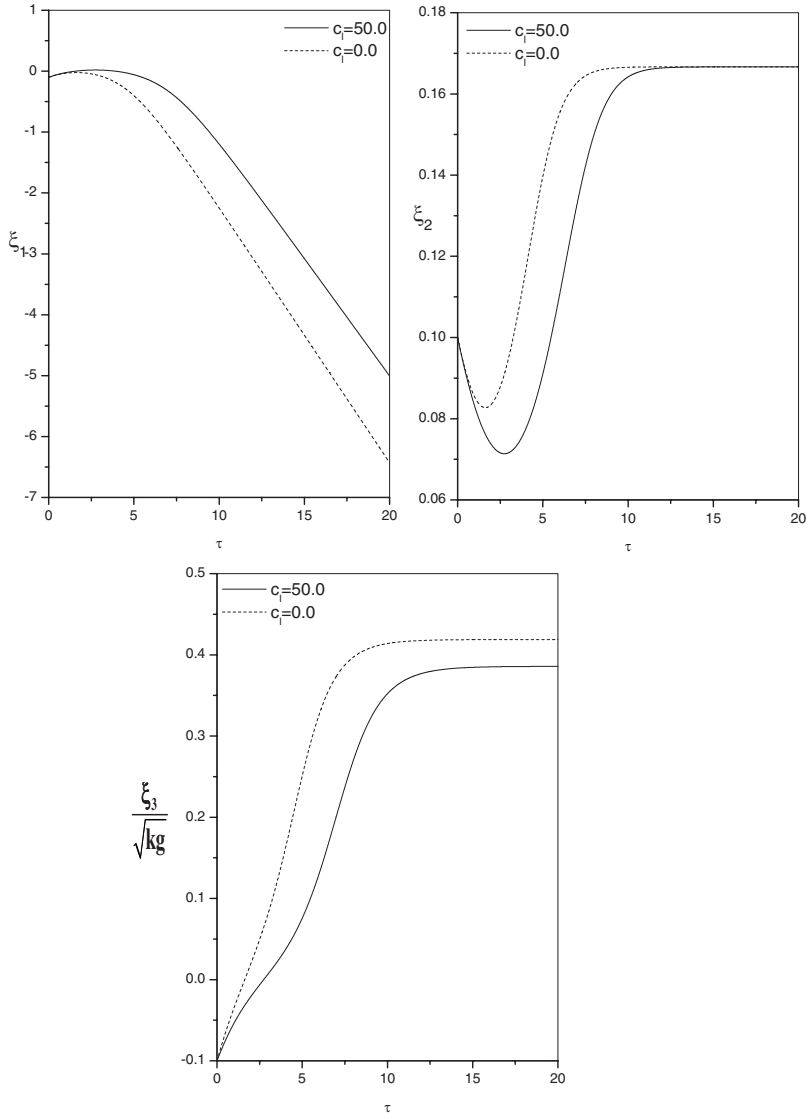

FIG. 4. The graph represents the solution of the set of equations (37), for spike; $\xi_1=-0.1$, $\xi_2=0.1$, $\xi_3/\sqrt{kg}=-0.1$, $\rho_{l1}(t=0)/\tilde{\rho}_{l0}=-0.001$ (compression), and $r^*=1.5262$. Growth rate reduction for spikes (RTI).

$$\rho_{h0}^*\left[-\frac{\partial\phi_h}{\partial t}+\frac{1}{2}(\nabla\phi_h)^2+gy\right]-\rho_{l0}^*\left[-\frac{\partial\phi_l}{\partial t}+\frac{1}{2}(\nabla\phi_l)^2+gy\right]$$
$$=-p_0\left[1-\frac{\rho_{h1}(t)}{\tilde{\rho}_{h0}}k^2\left(\xi_2+\frac{1}{2}\right)x^2\right]^{(\gamma_h-1)}$$
$$+p_0\left[1+\frac{\rho_{l1}(t)}{\tilde{\rho}_{l0}}k^2\left(\xi_2-\frac{1}{2}\right)x^2\right]^{(\gamma_l-1)}+\rho_{h0}^*f_h(t)-\rho_{l0}^*f_l(t), \tag{30}$$

$$\rho_{h0}^*=\frac{\gamma_h-1}{\gamma_h}\tilde{\rho}_{h0};\quad \rho_{l0}^*=\frac{\gamma_l-1}{\gamma_l}\tilde{\rho}_{l0}. \tag{31}$$

Equating the coefficient of x^2, i.e., to second degree in the transverse coordinate we get

$$\left\{\frac{\rho_{h0}^*}{\rho_{l0}^*}\left[-\frac{\partial\phi_h}{\partial t}+\frac{1}{2}(\nabla\phi_h)^2+gy\right]-\left[-\frac{\partial\phi_l}{\partial t}+\frac{1}{2}(\nabla\phi_l)^2+gy\right]\right\}$$
$$=\frac{p_0}{\rho_{l0}^*}\left[(\gamma_h-1)\frac{\rho_{h1}(t)}{\tilde{\rho}_{h0}}k\left(\eta_2+\frac{1}{2}k\right)\right.$$
$$\left.+(\gamma_l-1)\frac{\rho_{l1}(t)}{\tilde{\rho}_{l0}}k\left(\eta_2-\frac{1}{2}k\right)\right]. \tag{32}$$

Note that the left-hand side equated to zero yields the equation giving the acceleration $d\xi_3/dt$ of the tip of the bubble (spike) at the interface of the uniform density fluids, while the right-hand side represents the contribution to the acceleration due to compressibility and density inhomogeneity effects. Consequently, the resulting stabilization (or destabilization) of the interfacial structures determined by the corresponding growth rate is proportional to the unperturbed interfacial pressure p_0. Similar conclusion was arrived at by Livescu.[14]

After some straightforward algebraic manipulation retaining terms to $O(x^2)$, we finally obtain the following set of five equations [Eq. (33)] describing the dynamics of the tip of the bubble/spike. The first two equations are the same as Eqs. (11) and (12). We however include them here to make the set of equations look complete:

$$\frac{d\xi_1}{dt}=\xi_3,$$

$$\frac{d\xi_2}{dt}=-3\xi_3\left(\xi_2+\frac{1}{6}\right),$$

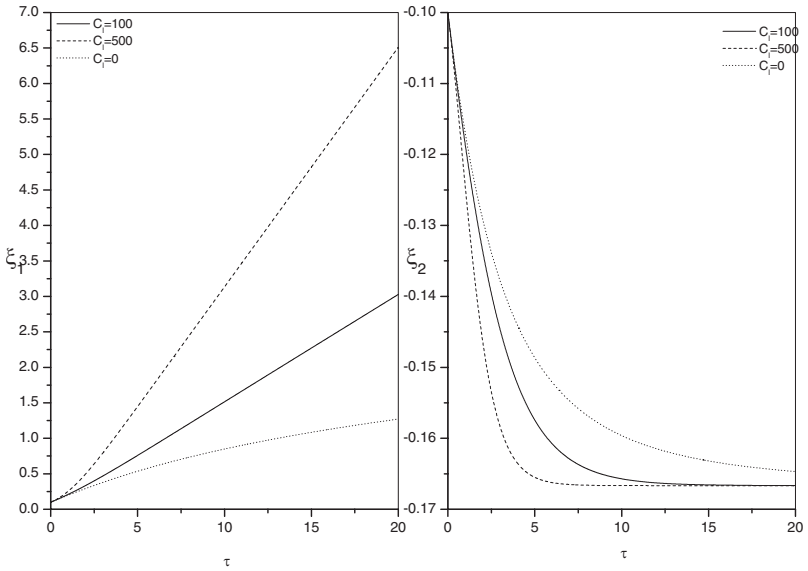

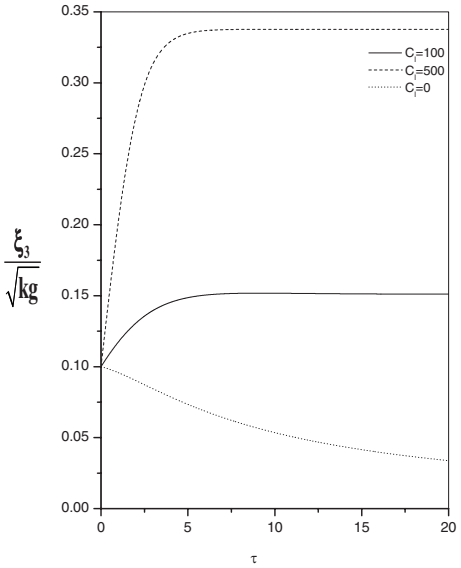

FIG. 5. Initial values same as in Fig. 1. $C_L=0$, 100, and 500; $\rho_{l1}(t=0)/\tilde{\rho}_{l0}=0.001$ (decompression), growth rate reduction (bubble) (RMI).

$$\frac{d\xi_3}{dt} = -\frac{N^*(\xi_2)}{D^*(\xi_2)}\frac{\xi_3^2}{6\xi_2-1} + 2kg(r^*-1)\frac{\xi_2(6\xi_2-1)}{D^*(\xi_2)} - \frac{1}{D^*(\xi_2)}k^2c_{sl}^2\left[\frac{\gamma_h-1}{\gamma_l-1}\frac{\rho_{h1}}{\tilde{\rho}_{h0}}\left(\xi_2+\frac{1}{2}\right) + \frac{\rho_{l1}}{\tilde{\rho}_{l0}}\left(\xi_2-\frac{1}{2}\right)\right], \tag{33}$$

$$\frac{1}{\rho_{h1}}\frac{d\rho_{h1}}{dt} = \frac{\xi_2-\frac{1}{2}}{\xi_2+\frac{1}{2}}\xi_3,$$

$$\frac{1}{\rho_{l1}}\frac{d\rho_{l1}}{dt} = \frac{\xi_2+\frac{1}{2}}{\xi_2-\frac{1}{2}}\frac{\xi_2+\frac{1}{6}}{\xi_2-\frac{1}{6}}\xi_3,$$

$$N^*(\xi_2) = 36(1-r^*)\xi_2^2 + 12(r^*+4)\xi_2 + (7-r^*),$$

$$D^*(\xi_2) = 12(1-r^*)\xi_2^2 + 4(1-r^*)\xi_2 + (1+r^*),$$

$$r^* = \rho_h^*/\rho_l^*, \tag{34}$$

$$\frac{\gamma_h-1}{\gamma_l-1} = r^*\frac{c_{sh}^2}{c_{sl}^2},$$

$$c_{sh}^2 = \frac{\gamma_h p_0}{\tilde{\rho}_{h0}}; \quad c_{sl}^2 = \frac{\gamma_l p_0}{\tilde{\rho}_{l0}}.$$

The set of equations (33) describes the time evolution of a bubble. To obtain the time evolution of a spike we have to make the transformation $\xi_1 \to -\xi_1$, $\xi_2 \to -\xi_2$ and $r \to 1/r$.[5]

For constant density fluids the instability development of bubble can be expressed as (ξ_3/k represents velocity)

$$\rho_l\frac{d\xi_3}{dt} = (\rho_h-\rho l)kgF(\xi_1) - \rho_l G(\xi_1)\xi_3^2, \tag{35}$$

where $F(\xi_1)=\xi_2(6\xi_2-1)/D(\xi_2)$ and $G(\xi_1)=N(\xi_2)/(6\xi_2-1)D(\xi_2)$ with $6\xi_2+1=\text{const}\exp(-3\xi_1)$; $N(\xi_2)$, $D(\xi_2)$ are the same as given in Eq. (34) with ρ_h^* and ρ_l^* replaced by ρ_h and ρ_l (for spike development ρ_h and ρ_l are to be interchanged).

It is interesting to note that Eq. (35) has the same form as that of the dynamical evolution equation in the buoyancy-drag phenomenological model for the instability of a two

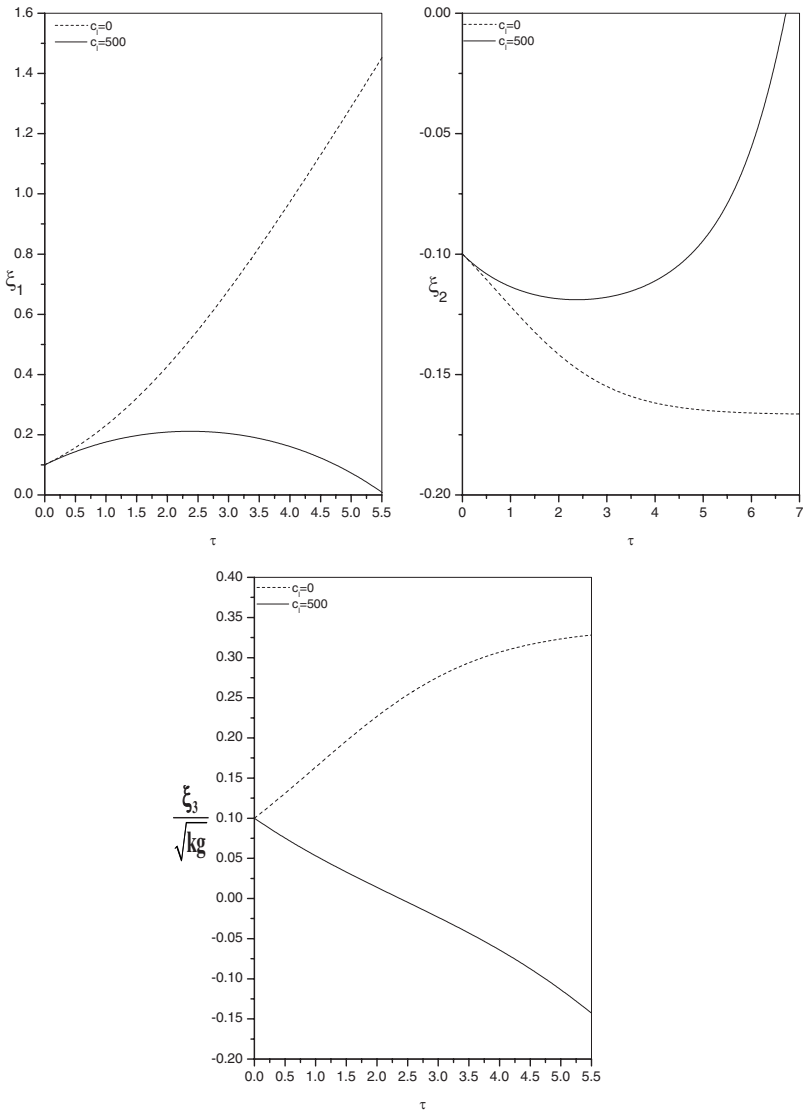

FIG. 6. The graph represents the solution of the set of equations (37) for $C_l=0$ and 500 considering initial values $\xi_1=0.1$, $\xi_2=-0.1$, $\xi_3/\sqrt{kg}=0.1$, $\rho_{l1}(t=0)/\tilde{\rho}_{l0}=-0.001$ (compression), and $r^*=1.5262$. The result shows growth rate (bubble) reduction.

fluid mixing front. The first term of the right-hand side of the above equation represents the force of buoyancy and the second one is the force due to drag.

IV. RESULTS AND DISCUSSIONS

For incompressible fluids (γ_h, $\gamma_l \to \infty$ and ρ_h, ρ_l constant) the results are known. Denoting the asymptotic velocity of the tip of the bubble or spike by $(\xi_3/k)_{\text{asymp}}$ we have the following:

$$\left(\frac{\xi_3}{k}\right)_{\text{asymp}} = \sqrt{\frac{2A}{3(1\pm A)}\frac{g}{k}} \quad \text{for RT bubble/spike},$$
$$\left(\frac{\xi_3}{k}\right)_{\text{asymp}} = \frac{1}{3}\left(1+\frac{2}{1\pm A}\right)\frac{1}{kt} \quad \text{for RM bubble/spike}. \tag{36}$$

Analytically closed form solution of the entire system of five equations [Eq. (33)] is not feasible; we have taken recourse to the method of numerical integration (fifth order Runge–Kutta–Fehlberg method). In order to assess the contribution of individual effects, e.g., the compressibility or density variation of either fluid we consider the following special cases.

A. Case (a)

Put $\rho_{h1}=0$. This substitution reduces the set of equations (33) to the following set of dimensionless form:

$$\frac{d\xi_1}{d\tau} = \frac{\xi_3}{\sqrt{kg}},$$
$$\frac{d\xi_2}{d\tau} = -3\frac{\xi_3}{\sqrt{kg}}\left(\xi_2+\frac{1}{6}\right),$$
$$\frac{d(\xi_3/\sqrt{kg})}{d\tau} = -\frac{N^*(\xi_2)}{D^*(\xi_2)}\frac{(\xi_3/\sqrt{kg})^2}{6\xi_2-1} + 2(r^*-1)\frac{\xi_2(6\xi_2-1)}{D^*(\xi_2)} - \frac{C_l}{D^*(\xi_2)}\frac{\rho_{l1}}{\tilde{\rho}_{l0}}\left(\xi_2-\frac{1}{2}\right), \tag{37}$$

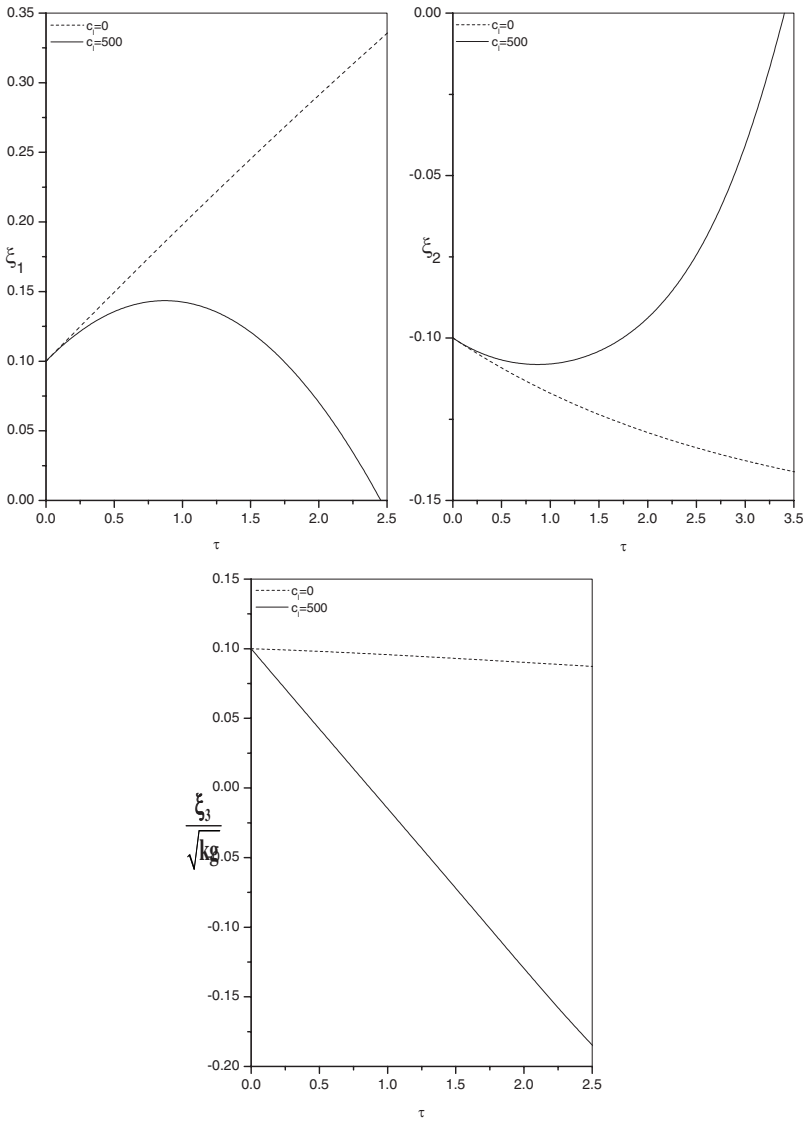

FIG. 7. The graph represents the solution of the set of equations (37), neglecting the second term of the third equation of the set (RMI), for $C_l=0$ and 500 considering initial values $\xi_1=0.1$, $\xi_2=-0.1$, $\xi_3/\sqrt{kg}=0.1$, $\rho_{l1}(t=0)/\tilde{\rho}_{l0}=-0.001$ (compression), and $r^*=1.5262$. The result shows growth rate (bubble) reduction.

$$\frac{1}{\rho_{l1}}\frac{d\rho_{l1}}{d\tau}=\frac{\xi_2+\frac{1}{2}}{\xi_2-\frac{1}{2}}\frac{\xi_2+\frac{1}{6}}{\xi_2-\frac{1}{6}}\frac{\xi_3}{\sqrt{kg}},$$

where

$$C_l=\frac{kc_{sl}^2}{g}=\frac{kp_0}{\rho_{l0}^* g}(\gamma_l-1),$$
$$\tau=t\sqrt{kg}. \tag{38}$$

The last equation in the set of equations (37) which governs the time evolution of $\rho_{l1}(t)$, shows that $\rho_{l1}<0(>0)$ according as $\rho_{l1}(0)<0(>0)$. Moreover, whether in the case of a bubble or spike $-1/6<\xi_2<1/6$; hence $\xi_2-\frac{1}{2}<0$. So by virtue of Eq. (24) according as $\rho_{l1}(t=0)>$ or <0 we have

$$\rho_l(x,y,t)=\tilde{\rho}_{l0}+k^2\rho_{l1}(t)\left(\xi_2-\tfrac{1}{2}\right)x^2<\tilde{\rho}_{l0}\quad\text{(decompression)},$$
$$\text{or}\quad>\tilde{\rho}_{l0}\quad\text{(compression)}. \tag{39}$$

Since $dA/d\rho_l<0$, the density of the overlying heavier fluid remaining unchanged the local Atwood number

$$A^*_{\text{local}}=\frac{\rho^*_{h0}-\rho^*_l(x,y,t)}{\rho^*_{h0}+\rho^*_l(x,y,t)}>\text{or}<A^*_0=\frac{\rho^*_{h0}-\rho^*_{l0}}{\rho^*_{h0}+\rho^*_{l0}} \tag{40}$$

according as there occurs decompression or compression. We have shown the results of numerical solution of set (37) for bubble ($\xi_1>0$, $\xi_2<0$) in Fig. 1 with $\rho_{l1}(t=0)>0$ which implies decompression of the lighter fluid according to relation (39) and so $A^*_{\text{local}}>A^*_0$. From the last inequality one would expect [see Eq. (36)] increase in instability growth rate (destabilization). This is exactly what we find in Fig. 1 which shows both ξ_1 and ξ_3 are greater than their values in absence of density variation ($C_l=0$). For spikes ($\xi_1<0$, $\xi_3>0$) the same results holds. This is shown in Fig. 2 (enhancement signified by increase in magnitude in $|\xi_1|$). On the other hand for $\rho_{l1}(t=0)<0$ which according to inequality (39) implies compression of the lighter fluid the results shown in Fig. 3 demonstrates that both ξ_1 and ξ_3 are less than their values corresponding to $C_l=0$ (i.e., stabilization for bubbles). This again is our theoretical expectation according to Eq. (36) as A^*_{local} is now $<A^*_0$. The same holds for spikes (Fig. 4).

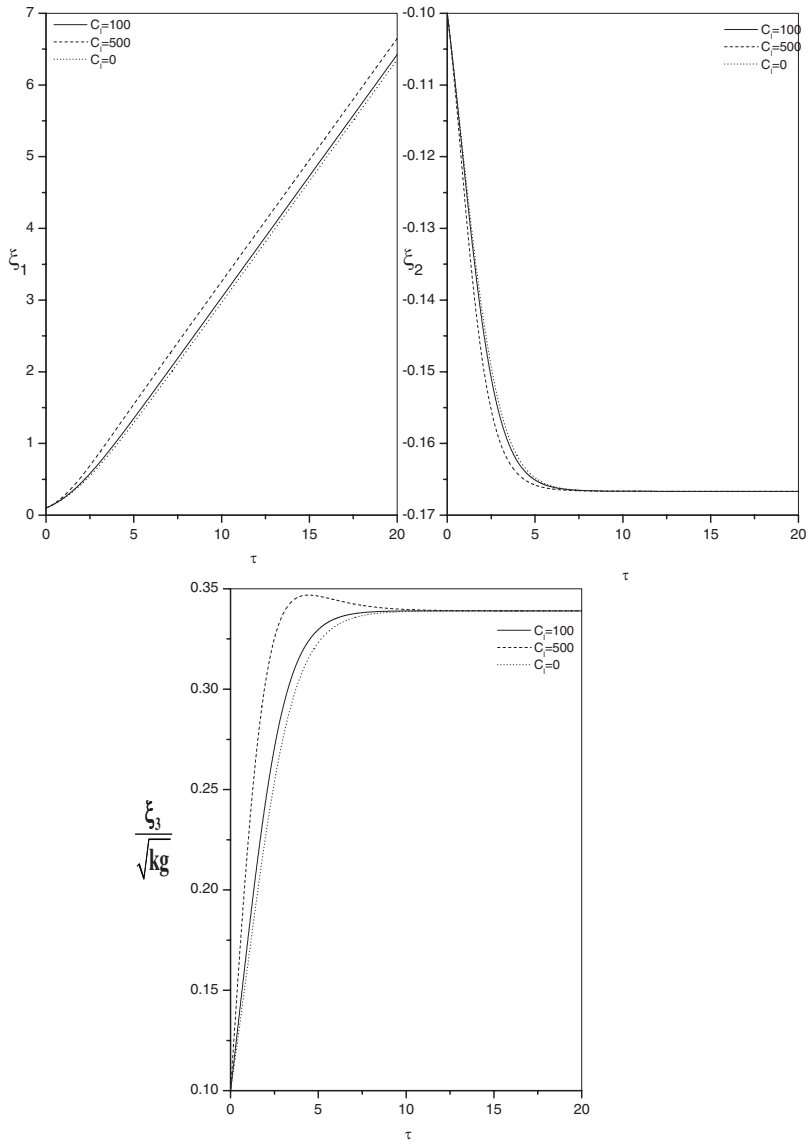

FIG. 8. The graph represents the solution of the set of equations (43) for $C_h=0$, 100, and 500 considering initial values $\xi_1=0.1$, $\xi_2=-0.1$, $\xi_3/\sqrt{kg}=0.1$, $\rho_{h1}(t=0)/\tilde{\rho}_{h0}=-0.001$ (compression), and $r^*=1.5262$. The result shows growth rate (bubble) enhancement.

The quantitative results and the associated discussions presented in the preceeding paragraphs apply equally well to bubble in the case of RMI determined by the solution of set (37) with the second term in its third member omitted. Outcomes similar to that in Fig. 1 are found to be true in Fig. 5. Similar conclusions hold for spike enhancement in RMI and also for RMI bubble and spike growth depression.

In case of RT instability an expression for approximate asymptotic value of the velocity of the tip of the bubble (spike) may be obtained provided

$$q_l(t)=\left(\xi_2-\frac{1}{2}\right)\int_0^{\infty}\frac{\rho_{l1}(\tau)}{\tilde{\rho}_{l0}}d\tau\rightarrow q_l(\infty),\quad \text{a constant} \tag{41}$$

as $t\rightarrow\infty$. For bubble (spike) $\xi_2\rightarrow -1/6$ (1/6) as $t\rightarrow\infty$. Under the above condition (41) the asymptotic value of ξ_3/k is obtained from Eq. (37) by equating $(d/d\tau)(\xi_3/k)$ to zero. This gives

$$(\xi_3/k)_{\text{asymp}}=\sqrt{\frac{2}{3}\frac{A^*}{1\pm A^*}\frac{g}{k}}\left[1+\frac{3}{2}\frac{1\mp A^*}{A^*}\frac{kc_{sl}^2}{g}q_l(\infty)\right]^{1/2}. \tag{42}$$

The upper (lower) sign corresponds to bubble (spike). The numerical results given in Figs. 1–4 are in support of Eq. (42). However the last equation does not hold if $\xi_2>0$ in the case of a bubble or to $\xi_2<0$ in case of a spike [Eqs. (2) and (3)].

It is in order to note here that if we are interested in the growth rate of the bubble, it follows from Eq. (2) that it is not meaningful to follow the numerical integration beyond the stage to $\xi_2>0$ through $\xi_2=0$. For spikes the restriction applies to the stage to $\xi_2<0$ through $\xi_2=0$ [Eq. (3)]. This is what is done in Figs. 6 and 7.

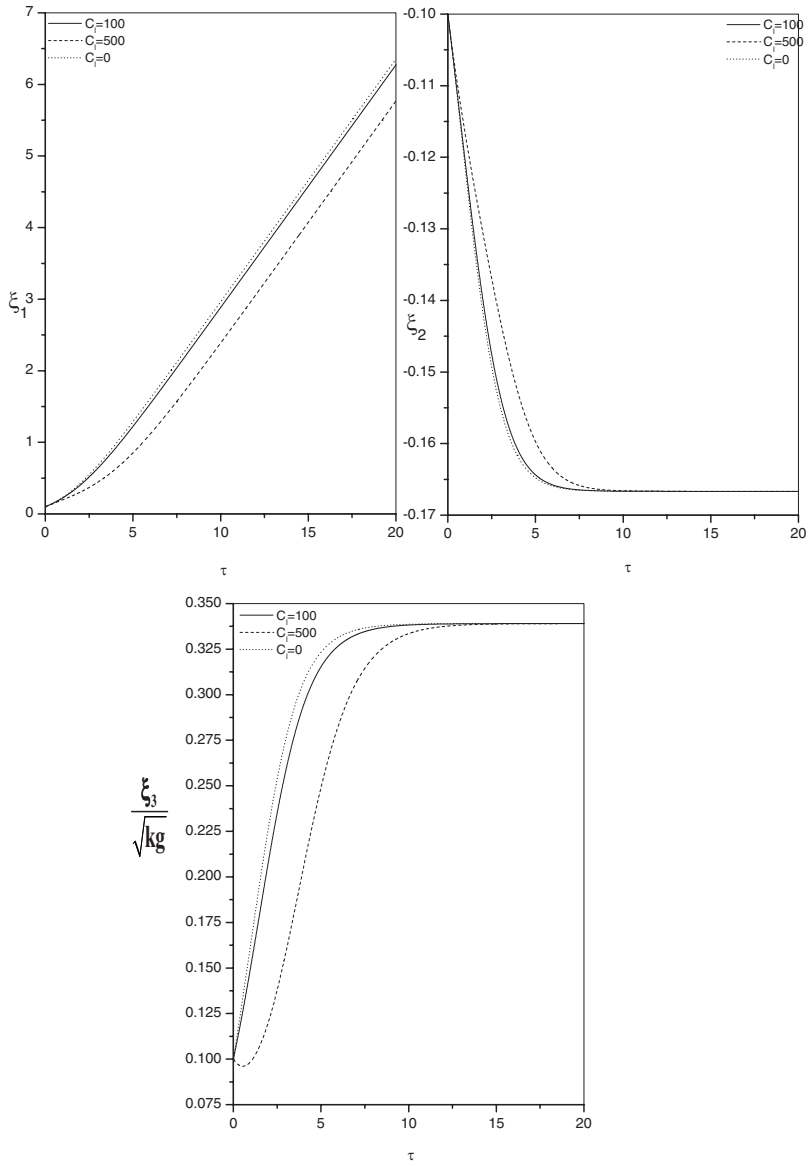

FIG. 9. The graph represents the solution of the set of equations (43) for $C_h=0$, 100, and 500 considering initial values $\xi_1=0.1$, $\xi_2=-0.1$, $\xi_3/\sqrt{kg}=0.1$, $\rho_{h1}(t=0)/\tilde{\rho}_{h0}=0.001$ (decompression), and $r^*=1.5262$. The result shows growth rate (bubble) reduction.

B. Case (b)

Put $\rho_{l1}=0$. This substitution reduces set (33) to the following dimensionless form:

$$\frac{d\xi_1}{d\tau}=\frac{\xi_3}{\sqrt{kg}},$$

$$\frac{d\xi_2}{d\tau}=-3\frac{\xi_3}{\sqrt{kg}}\left(\xi_2+\frac{1}{6}\right),$$

$$\frac{d(\xi_3/\sqrt{kg})}{d\tau}=-\frac{N^*(\xi_2)}{D^*(\xi_2)}\frac{(\xi_3/\sqrt{kg})^2}{6\xi_2-1}+2(r^*-1)\frac{\xi_2\left(\xi_2-\frac{1}{6}\right)}{D^*(\xi_2)}-\frac{C_h}{D^*(\xi_2)}\frac{\rho_{h1}}{\tilde{\rho}_{h0}}\left(\xi_2+\frac{1}{2}\right), \tag{43}$$

$$\frac{1}{\rho_{h1}}\frac{d\rho_{h1}}{d\tau}=\frac{\xi_2-\frac{1}{2}}{\xi_2+\frac{1}{2}}\frac{\xi_3}{\sqrt{kg}}$$

where

$$C_h=\frac{kp_0}{\rho_{l0}^*g}(\gamma_h-1)=r^*\frac{kc_{sh}^2}{g}. \tag{44}$$

The last equation in the set of equations (43) which governs the time evolution of $\rho_{h1}(t)$ shows that $\rho_{h1}<0$ or >0 according as $\rho_{h1}(t=0)<0$ or >0. On employing Eq. (20) we find that $\rho_h^*(x,y,t)>$ or $<\rho_{h0}^*$ according as $\rho_{h1}^*(0)$ is <0 or >0. Since $dA/d\rho_h>0$ the preceding inequality has the consequence that local Atwood number $[\rho_h^*(x,y,t)-\rho_{l0}^*]/[\rho_h^*(x,y,t)+\rho_{l0}^*]$ is $>$ or $<A_0^*=(\rho_{h0}^*-\rho_{l0}^*)/(\rho_{h0}^*-\rho_{l0}^*)$ according as $\rho_{h1}(0)$ is <0 or >0. Thus growth rate is lowered when $\rho_{h1}(0)>0$ (decompression of the heavier fluid ρ_h) and enhanced when $\rho_{h1}(0)<0$ (compression of heavier fluid). These theoretically expected results are seen to agree with the numerical ones of Figs. 8 and 9.

C. Case (c)

We next turn our investigation to the study of the effect of compressibility, (the finiteness of the value of γ_h and γ_l) assuming both $\rho_{h1}(0)\approx 0$ and $\rho_{l1}(0)\approx 0$ so that the third term in the equation for dx_3/dt in the set of equations (33) may be ignored. This is equivalent to assuming the density variation to be negligibly small. The asymptotic expression for the velocity of the tip of the nonlinear structures is then given by

$$(\xi_3/k)_{\text{asymp}} = \sqrt{\frac{2}{3}\frac{A^*}{1\pm A^*}\frac{g}{k}} \quad \text{for RTI,}$$
$$(\xi_3/k)_{\text{asymp}} \approx \frac{1}{3}\left(1+\frac{2}{1\pm A^*}\right)\frac{1}{kt} \quad \text{for RMI.} \tag{45}$$

First take $\gamma_h\to\infty$ (heavier fluid incompressible) and γ_l finite so that $\rho^*_{h0}=\tilde{\rho}_{h0}$ and $\rho^*_{l0}=[1-(1/\gamma_l)]\tilde{\rho}_{l0}$. Thus ρ^*_{l0} increases as γ_l increases and since $dA/d\rho_l<0$ Atwood number $A^*=(\rho^*_{h0}-\rho^*_{l0})/(\rho^*_{h0}+\rho^*_{l0})$ decreases as ρ^*_{l0} increases. Using Eq. (45) we find that the velocity of the tip of the bubble (as well as that of the spike) decreases. Thus the growth rate decreases as γ_l increases and ultimately merges to the limiting value for incompressible fluid ($\gamma_h\to\infty$ and $\gamma_l\to\infty$).

On the other hand it can be easily shown by following the same line of argument with $\gamma_l\to\infty$ that as $(dA/d\rho_h>0)$ we have $A^*>A$ so that the growth rate increases as γ_h increases $[\rho^*_{h0}=[1-(1/\gamma_h)]\tilde{\rho}_{h0}]$ and $\to$ the incompressible fluid limiting value as $\gamma_h\to\infty$ and $\gamma_l\to\infty$.

If $\tilde{\rho}_{h0}>\tilde{\rho}_{l0}$ but $\gamma_h<\gamma_l$ then $A^*=(\rho^*_h-\rho^*_l)/(\rho^*_h+\rho^*_l)<A=[(\tilde{\rho}_{h0}-\tilde{\rho}_{l0})/(\tilde{\rho}_{h0}+\tilde{\rho}_{l0})]$ so that in this case compressibility reduces instability (e.g., for SF_6-air) while if $\gamma_h>\gamma_l$ (e.g., for Au-foam) we have $A^*>A$ and consequently compressibility will have the opposite effect, i.e., instability is enhanced. Thus depending on the relative magnitude of γ_h and γ_l compressibility has different roles to play regarding stabilization. The possibility of such varying influence of compressibility on stabilization agrees with the earlier linear theory RTI.[9] Here we find that identical conclusions are true for RMI.

D. Case (d)

Finally we discuss the dependence of growth rates on the wave number k and surface pressure p_0. In all Figs. 1–5, 8, and 9 it is seen that the magnitude of the enhancement or instability depends on the constants $C_l=kc^2_{sl}/g$ or $C_h=kc^2_{sh}/g$. These coefficients in their turn are proportional to kp_0. If the lighter fluid is decompressed it is seen from Figs. 1, 2, and 5 that growth rate enhancement increases with increase in the product kp_0, while if it is compressed (Figs. 3 and 4), the growth rate reduction increases with increase in kp_0. On the other hand in case of the heavier fluid the opposite results are true (Figs. 8 and 9); the role of compression and decompression are interchanged.

V. SUMMARY

Finally we briefly summarize the results.

(i) The density of the heavier fluid remaining unchanged the growth rate is enhanced (destabilization) when the lighter fluid is decompressed. While it is suppressed (stabilization) when the lighter fluid is compressed. The result is in agreement with theoretical expectation as decompression of the lighter fluid leads to raising and compression leads to lowering of the value of the Atwood number [Eq. (37)]. Asymptotic expression for the velocity of the bubble (spike) is given by Eq. (42).

(ii) The density of the lighter fluid remaining unchanged the growth rate is enhanced (destabilization) when the heavier fluid is compressed. While it is suppressed (stabilization) when the heavier fluid is decompressed. Here also there exists agreement with theoretical expectation as compression/decompression of the heavier fluid has the consequence that the Atwood number is increased/decreased.

(iii) Assuming density variation to be negligibly small and that γ_h, the ratio of specific heat of the heavier fluid remains unchanged the growth rate increases as γ_l decreases. The result is reversed when γ_l remains unchanged and γ_h decreases.

(iv) Once again with $\tilde{\rho}_{h0}>\tilde{\rho}_{l0}$ and with negligible density variation if $\gamma_h<\gamma_l$ (SF_6-air) there occurs reduction in instability while if $\gamma_h>\gamma_l$ (Au-foam) there occurs enhancement.

(v) The magnitude of destabilization or stabilization measured by the change in the magnitude of the nondimensional velocity $(\xi_3/\sqrt{kg})$ due to fluid density variation is an increasing function of the interfacial pressure p_0 and also of the wave number k.

ACKNOWLEDGMENTS

The authors are thankful to the referee for suggesting improvement in the presentation.

[1] J. Hecht, U. Alon, and D. Shavrts, Phys. Fluids **6**, 4019 (1994).
[2] A. L. Velikovich and G. Dimonte, Phys. Rev. Lett. **76**, 3112 (1996).
[3] G. Hazak, Phys. Rev. Lett. **76**, 4167 (1996).
[4] Q. Zhang, Phys. Rev. Lett. **81**, 3391 (1998).
[5] V. N. Goncharov, Phys. Rev. Lett. **88**, 134502 (2002).
[6] P. Sohn, Phys. Rev. E **67**, 026301 (2003).
[7] D. Layzer, Astrophys. J. **122**, 1 (1955).
[8] V. N. Goncharov and D. Li, Phys. Rev. E **71**, 046306 (2005).
[9] A. M. Lezzi and A. Prosperetti, Phys. Fluids A **1**, 1784 (1989).
[10] I. B. Bernstein and D. L. Book, Phys. Fluids **26**, 453 (1983).
[11] L. Baker, Phys. Fluids **26**, 950 (1983).
[12] M. S. Plesset and D. Hsieh, Phys. Fluids **7**, 1099 (1964).
[13] M. S. Plesset and A. Prosperetti, Phys. Fluids **25**, 911 (1982).
[14] D. Livescu, Phys. Fluids **16**, 118 (2004).
[15] B. Cheng, J. Glimm, and D. H. Sharp, Phys. Rev. E **66**, 036312 (2002).
[16] G. Dimonte and M. Schneider, Phys. Fluids **12**, 304 (2000).
[17] G. Dimonte, Phys. Plasmas **7**, 2255 (2000).
[18] R. P. Drake, *High Energy—Density Physics* (Springer, New York, 2006), p. 175.